




Strong gravitational lensing, quasi-periodic oscillations and constraints from EHT observations for quantum-improved charged black hole

Niyaz Uddin Molla^{1,a}, Himanshu Chaudhary^{2,3,4,b}, G. Mustafa^{5,6,c}, Ujjal Debnath^{1,d}, S. K. Maurya^{7,e} 

¹ Department of Mathematics, Indian Institute of Engineering Science and Technology, Shibpur, Howrah 711 103, India

² Pacif Institute of Cosmology and Selfology (PICS), Sagara, Sambalpur 768224, Odisha, India

³ Department of Applied Mathematics, Delhi Technological University, Delhi 110042, India

⁴ Department of Mathematics, Shyam Lal College, University of Delhi, Delhi 110032, India

⁵ Department of Physics, Zhejiang Normal University, Jinhua 321004, People's Republic of China

⁶ New Uzbekistan University, Movarounnahr street 1, Tashkent 100000, Uzbekistan

⁷ Department of Mathematical and Physical Sciences, College of Arts and Sciences, University of Nizwa, Nizwa 616, Sultanate of Oman

Received: 5 February 2024 / Accepted: 13 March 2024 / Published online: 12 April 2024
© The Author(s) 2024

Abstract We investigate strong gravitational lensing by quantum-improved charged black holes characterized by an additional parameter denoted as ω , in addition to the mass M and charge Q . Our findings reveal that when both the parameters $Q/2M$ and $\omega/4M^2$ increase simultaneously, various astrophysical consequences, such as the deflection angle $\alpha_D(u)$ and angular image separation increase. Concurrently, the angular position θ_∞ , relative magnification r_{mag} , and the time delay $\Delta T_{2,1}$ between the first and second relativistic images also decrease with the growing values of the parameters $Q/2M$ and $\omega/4M^2$. It is also observed that the Einstein ring θ_1^E for the quantum-improved charged black hole is more significant than those for Schwarzschild, quantum-improved Schwarzschild, and Reissner–Nordström black holes. As with supermassive black holes such as $M87^*$ and $SgrA^*$, it is observed that to be a viable astrophysical black hole, the EHT results constrain the parameter space $(\omega/4M^2, Q/2M)$. Remarkably, the EHT results for $SgrA^*$ impose more stringent limits on the parameter space of quantum-improved charged black holes compared to those established by the EHT results for $M87^*$. We investigate the radial profiles of orbital and radial harmonic oscillation frequencies as a function of the dimensionless coupling constants and black hole mass. The main characteristics of test particle quasi-periodic

oscillations close to stable circular orbits in the black hole equatorial plane are also examined. We study the positioning of resonant radii in the background of quantum-improved charged black holes for high-frequency quasi-periodic oscillations models: warped disc (WD) models, relativistic precession (RP) and its types, and epicyclic resonance (ER) and its variants.

1 Introduction

Investigating black holes through astrophysical observations is one of the most significant missions in the realms of gravitational and cosmological physics. This undertaking holds paramount significance, offering profound insights into the fundamental nature of these mysterious cosmic entities. The gravitational and cosmological implications associated with black holes make them a central focus for scientists striving to attain a deeper understanding of the universe. The detection of $GW150914$ by the LIGO and Virgo Collaborations marked the first observation of a gravitational wave event resulting from the merger of a binary system of black holes [1]. Additionally, the Event Horizon Collaboration released an image capturing the shadow of the black hole situated at the center of the galaxy $M87$ [2]. These observations serve as crucial evidence, motivating further exploration into the properties of black holes. Observable quantum fluctuations influence their geometries. However, the existence of singularities, where spacetime density becomes infinitely large, poses a challenge. The conflict between the profound impli-

^a e-mail: niyazuddin182@gmail.com

^b e-mail: himanshuch1729@gmail.com

^c e-mail: gmustafa3828@gmail.com (corresponding author)

^d e-mail: ujjaldebnath@gmail.com

^e e-mail: sunil@unizwa.edu.om (corresponding author)

cations of general relativity in astronomy and the limitations arising from the non-applicability of quantum physics concepts continues to be a significant impediment to understanding black hole physics. In recent years, remarkable progress has been made in black hole physics. However, there is a need for more in-depth exploration into the significant and intriguing characteristics of black holes, with a particular focus on their formation of relativistic images. Notable features such as gravitational lensing [3], shadows [4], quasinormal modes [5] play a vital role in advancing our understanding of general relativity, modified theories of gravity, quantum gravity, and quantum mechanics. Unfortunately, observing these features of black holes presents substantial challenges, given the constraints of technical limitations and the stringent requirements for theoretical accuracy. Scientists have increasingly come to appreciate the significance of quantum gravity effects in the proximity of singularities. There is a strong consensus that the elimination of singularities requires the incorporation of a quantum theory of gravity, given their exceedingly high energy density and curvature [6]. While awaiting the development of a self-consistent and widely accepted quantum theory of gravity, various approaches have been explored. These include transforming singularities into regular cores [7,8], leveraging quantum pressure to prevent the collapse of matter and induce a bounce [9,10], and eliminating event horizons through the creation of quasi-black holes [10–13]. Hence, a black hole could be inherently quantum, leading to the manifestation of quantum gravitational effects near the event horizons [14,15]. This occurrence is attributed to quantum fluctuations [16], proposing the concept of a fuzzball [17], or considering it as an exotic compact object [18,19]. These quantum features offer resolutions to the long-standing information loss paradox. Theoretical exploration of a quantum theory of gravity, encompassing models like M-theory, string theory, or loop quantum gravity, has been a focus of substantial research. A comprehensive quantum gravity framework was discussed in [20], wherein a scale-dependent action was introduced, and an exact renormalization group equation was derived. This contribution represents a noteworthy advancement in understanding the intricate dynamics of quantum gravity near singularities. By employing the renormalization group equation on the Einstein-Hilbert truncation, one can derive a non-perturbative estimate of the renormalization group flow for the Newton and cosmological constants. Previous investigations have incorporated the influence of matter fields [21–24]. An important characteristic of the non-perturbative quantum gravity method is the presence of a non-Gaussian fixed point in its renormalization group flow. This fixed point is crucial in the asymptotic safety scenario, rendering quantum gravity non-perturbatively renormalizable [25,26]. A powerful approach for determining quantum corrections to general relativity and quantum Einstein gravity solutions is through

the precise renormalization group flow equation [27–31]. An extensively studied concept in the literature is the renormalization group improved Schwarzschild black hole [32]. The central idea involves the “renormalization group improvement” of the Schwarzschild spacetime by incorporating the running Newton constant, a concept borrowed from standard particle physics schemes. This modification eliminates the classical singularity at the center of a Schwarzschild black hole, replacing it with a de Sitter core due to quantum effects. In a recent investigation, Ruiz and Tuiran [32] delved into the implications of running Newton’s constant on various essential features of spherically symmetric charged black holes. They achieved this by undertaking a renormalization group improvement of the classical Reissner-Nordström metric. This study was performed using the Einstein-Hilbert truncation method within the context of quantum Einstein gravity. Various aspects of its black hole physics, such as the number of horizons, regularity, critical mass, and thermodynamics [26], as well as its quantum gravitational effects on accretion [33], have been extensively studied. Recently, both weak and strong deflection gravitational lensing by a renormalization group improved Schwarzschild’s black hole and was explored in [34]. However, the impact of the quantum correction parameter on the physical characteristics of the charged black hole, particularly in terms of strong gravitational lensing and the signatures of quasi-periodic oscillations (QPOs), remains unexplored in the existing literature. In the present paper, we intend to study strong gravitational lensing and the QPOs of massive particles near the circular orbit in the context of a quantum-improved charged black hole.

Gravitational lensing, a consequence of Einstein’s general relativity, plays a foundational and influential role in astrophysics, offering a robust method to probe the strong-field nature of gravity. This phenomenon serves as a potent tool for magnifying and examining distant celestial objects, providing astronomers with heightened observations of galaxies and quasars and facilitating the detection of elusive entities such as dark matter, dark energy, and gravitational waves. Additionally, it contributes to the comprehensive study of various astronomical phenomena [35,36]. The distortion of the image of black holes with a gridding accretion fragment results from the strong gravitational lensing effect. Initially, astronomers measured the deflection angle caused by the sun during a solar eclipse [37]. However, such observations were realistically only feasible with the sun. A shift in perspective occurred with the groundbreaking ideas of Fritz Zwicky, who proposed the possibility of observing lensing effects caused by galaxies and even clusters of galaxies. Various approaches have been proposed to investigate gravitational lensing around black holes, covering weak and strong field limits. Light closely approaches the source in strong gravitational lensing, where the gravitational field is sufficiently

intense, leading to significant bending angles. This results in diverse paths that light can take to reach the observer, potentially generating multiple images, arcs, and rings of the source. Phenomena such as shadows, photon rings, and relativistic images may manifest in these scenarios [38–40]. Several studies have investigated the exploration of gravitational lensing in the strong field limits around black holes over the past few years [41–44].

In astrophysics, the identification of quasiperiodic oscillations (QPOs) in X-ray emissions from neutron stars and black holes opens a window into the extreme gravitational environments surrounding these celestial objects. The periodic fluctuations in luminosity indicate the existence of underlying physical processes, such as oscillations of accretion disks or gravitational interactions, serving as valuable probes for exploring the fundamental nature of spacetime. The detection of QPOs in accretion disks around black holes implies the existence of resonant oscillations that may be associated with the innermost stable circular orbits, furnishing valuable insights into the strong gravity regime and creating opportunities to test Einstein’s theory of general relativity. After the initial discovery of QPOs during the analysis of X-ray binary spectra and flux [45], numerous studies have been dedicated to exploring the theoretical aspects of QPOs and their nature. Among the prominent models explaining QPO is the one related to particle dynamics and the corresponding oscillations of their trajectories. From this standpoint, investigations into QPOs arising from the collective motion of charged particles within accretion disks have been conducted in a series of works [46,47]. High-frequency QPOs with dual peaks that nearly fit the ratio are commonly seen in black hole microquasars [48]. High-frequency QPOs of neutral [49], spinning [50], and charged test particles [51] in the proximity of rotating and non-rotating black holes have been the subject of numerous investigations. Hot-spot data surrounding Sgr A* have been used recently to investigate alternate rotating spacetimes [52]. Recently, Liu et al. [53] discussed the Orbital motion and QOPS with periastron and Lense-Thirring precession in the background of a slowly rotating Einstein-Æther black hole. In another study, [54] investigated the Kerr black hole with quintessential dark energy through observational data using QOPS and its different invariants.

The aim of this study is to explore the astrophysical implications of quantum-improved charged black holes via strong gravitational lensing. Additionally, we aim to extend the applications of these findings to describe Quasiperiodic Oscillations (QPOs). This paper is organized as follows: In Sect. 2, we discuss the strong gravitational lensing and its various astrophysical consequences due to the quantum-improved charged black hole. Furthermore, we study the quasiperiodic oscillations of massive particles near the circular orbit in Sect. 3. We also test the high-frequency QPOs models in Sect. 4. Finally, we present some concluding

remarks in the last Sect. 5. We use natural units $G_0 = c = 1$ throughout the paper unless the units are specifically defined.

2 Strong gravitational lensing by Quantum-improved charged black hole

The renormalization group flow equation (ERGE) serves as a theoretical tool, offering a non-perturbative method to explore quantum corrections to the precise solutions of the Einstein field equations. The foundation of this concept lies in the assumption that the general theory of relativity operates as an effective theory at lower energy levels, stemming from a more fundamental theory applicable at higher energy scales [20]. The term “quantum Einstein gravity (QEG)” denotes this fundamental theory and its ensuing implications. Regarding the search for non-perturbative quantum corrections to Einstein gravity, researchers have investigated three potential levels of enhancement thus far [26,29,30,55]. At the first level, the process directly replaces the relevant running couplings within the metric components. At the second level, this substitution occurs within the field equations. The third level, characterized by the highest deductive power, entails directly substituting the running couplings into the action. Ruiz and Tuiran [32] exclusively explored the impact of running Newton’s constant, and they implemented improvements at the foundational first level. Numerous earlier findings on the quantum improvement of classical black hole spacetimes establish direct or indirect connections with the Reissner-Nordström solution. Specifically, Ruiz and Tuiran pursued further exploration in subsequent studies [26,55,56]:

- (i) Numerous expressions obtained for the improved Schwarzschild black hole strikingly parallel the corresponding expressions observed in the classical Reissner-Nordström spacetime.
- (ii) The original formulation of the first law of black hole mechanics is disrupted in the context of the enhanced Kerr spacetime, leading to a departure from the direct proportionality between Hawking temperature and surface gravity.
- (iii) The evaluation of the Komar integral for the mass of the improved Schwarzschild and Kerr black holes reveals an antiscreening effect associated with the gravitational quantum field.

The above-mentioned results serve as pivotal points for the quantum improvement of classical black hole spacetimes, particularly in the context of the Reissner-Nordström (RN) solution. The Reissner-Nordström solution characterizes a spherically symmetric spacetime and is represented by the

metric

$$ds^2 = -f(r)dt^2 + \frac{1}{f(r)}dr^2 + r^2d\Omega^2, \tag{1}$$

with the function

$$f(r) = 1 - \frac{2G_0M}{r} + \frac{G_0Q^2}{r^2}. \tag{2}$$

where, $d\Omega^2 \equiv d\theta^2 + \sin^2\theta d\phi^2$ represents the infinitesimal element of squared solid angle, G_0 represents Newton’s gravitational constant, M signifies the mass of the black hole, Q denotes the charge of the black hole. Assuming as a principal hypothesis that beyond the classical limit, the primary effects of quantum gravity, particularly related to linear fluctuations of the metric for sufficiently long distances, are incorporated in the dependence of Newton’s constant on the energy scale or the renormalization group (RG) infrared cutoff k [57]; and identifying the cutoff k with the inverse of a scalar proper distance $d(r)$, where $k = \xi/d(r)$, the resulting improved Reissner-Nordström geometry is expressed as follows:

$$ds^2 = -f_I(r)dt^2 + \frac{1}{f_I(r)}dr^2 + r^2d\Omega^2; \tag{3}$$

$$f_I(r) = 1 - \frac{2G(r)M}{r} + \frac{G(r)Q^2}{r^2}. \tag{4}$$

where the superscript ‘ I ’ stands for ‘improved,’ and the running Newton’s constant is given by:

$$G(k) \equiv \frac{G_0}{1 + \bar{\omega}G_0k^2}, \tag{5}$$

and

$$G(r) \equiv G\left(k = \frac{\xi}{d(r)}\right) = \frac{G_0d^2(r)}{d^2(r) + \omega G_0}. \tag{6}$$

where $\omega \equiv \bar{\omega}\xi^2$ is a free parameter that toggles the quantum effects ‘on’ and ‘off’. Equations 3 and 5 are applicable, as previously mentioned, to distances that are significantly larger than the Planck length, denoted as $l_p = \sqrt{\frac{\hbar G_0}{c^3}}$. Ruiz and Tuiran [32] devoted their investigation to the specific quantum corrections applied to the classical black hole model. They provided detailed mathematical formulations and principles guiding these corrections. Additionally, they explicitly highlighted how these corrections lead to introducing the parameter ω . Quantum-improved charged black holes constitute a theoretical framework that integrates the principles of quantum mechanics and general relativity, aiming to enhance our comprehension of the unique characteristics displayed by charged black holes. The static spherically symmetric Quantum-improved charged black hole is described by [32,58]

$$ds^2 = \left(1 - \frac{2G_0rM}{G_0\omega + r^2} + \frac{G_0Q^2}{G_0\omega + r^2}\right) dt^2$$

$$- \left(1 - \frac{2G_0rM}{G_0\omega + r^2} + \frac{G_0Q^2}{G_0\omega + r^2}\right)^{-1} dr^2 - r^2d\theta^2 - r^2\sin^2\theta d\phi^2 \tag{7}$$

where the parameter ω serves as the quantum parameter, measuring quantum effects arising from non-perturbative renormalization group considerations. The parameter ω in the context of a quantum-improved charged black hole plays a crucial role in influencing the quantum corrections applied to the classical black hole model. The physical interpretation of ω in the context of a quantum-improved charged black hole is as follows:

- The new parameter ω cannot be exclusively derived from renormalization group arguments. In principle, it should be experimentally determined by measuring the quantum correction to the Newton potential [59,60]. It possesses some properties, defining it as a suitable parameter to activate or deactivate quantum effects such as
 - (a) ω is proportional to the Planck constant \hbar ,
 - (b) ω is the only constant in Eq. 6 associated with the evolution of G with the scale k ,
 - When $\omega = 0$, the standard value of Newton’s constant is restored, i.e. $G(k) = G_0$.
- ω is a parameter that characterizes the quantum corrections applied to the classical black hole solution. It is associated with the introduction of quantum effects into the gravitational field. The value of ω determines the strength and nature of these quantum corrections.
- In certain theoretical frameworks, ω is linked to scalar fields that can emerge from quantum field theory. The scalar field may represent additional degrees of freedom in the gravitational field, contributing to the quantum aspects of the black hole.
- The parameter ω serves as a modulator for the quantum corrections incorporated into the black hole metric. Its presence influences the behavior of the running Newton’s constant and other relevant parameters, thereby shaping the quantum-improved charged black hole solution and determining the extent of departure from classical predictions.

Various choices of these physical parameters lead to distinct spacetimes, as follows: The spacetime (7) reduces to that of the Schwarzschild black hole if $\omega = 0 = Q$; quantum-improved Schwarzschild black hole [31] if $Q = 0$; Reissner-Nordström black hole if $Q \neq 0, \omega = 0$; and the quantum-improved charged black hole [32,58] when $Q \neq 0, \omega \neq 0$. In this section, we discuss the strong gravitational lensing and its various observables for the quantum-improved charged black hole and compare the results with the cases of Schwarzschild

black hole, quantum-improved Schwarzschild and Reissner-Nordström black hole.

2.1 Equatorial lensing

Here, we discuss the deflection of photon rays in the equatorial plane ($\theta = \frac{\pi}{2}$) due to Quantum-improved charged black hole. To obtain the strong deflection angle of a light ray in the equatorial plane ($\theta = \frac{\pi}{2}$) of a black hole, we rewrite the metric (7) by redefining the quantities r, t, ω and Q in units of the radius $2M$, so that $t \rightarrow t/2M, r \rightarrow r/2M, \omega \rightarrow \omega/4M^2$ and $Q \rightarrow Q/2M$, respectively

$$d\bar{s}^2 = -A(r)dt^2 + B(r)dr^2 + C(r)(d\theta^2 + \sin^2\theta d\phi^2), \tag{8}$$

where

$$A(r) = 1 - \frac{G_0 r}{r^2 + G_0 \omega} + \frac{G_0 Q^2}{r^2 + G_0 \omega} \tag{9}$$

$$B(r) = \left(1 - \frac{G_0 r}{r^2 + G_0 \omega} + \frac{G_0 Q^2}{r^2 + G_0 \omega}\right)^{-1} \tag{10}$$

$$C(r) = r^2. \tag{11}$$

Gravitational lensing in the strong field regime is determined by the interplay of the deflection angle and the lens equation. The null geodesic equation can be expressed as follows

$$\dot{r} = \frac{dr}{d\tau} = \sqrt{E^2 - \frac{L^2}{r^2} A(r)}, \tag{12}$$

where the constants E and L are the energy and the angular momentum of the particle, τ is the affine parameter along the geodesics, while the function $A(r)$ is given by Eq. (9). Introducing the ratio $\frac{E}{L}$ as an impact parameter denoted by u , the above Eq. (12) can be expressed [61]

$$\dot{r}^2 + V_{eff} = 0 \tag{13}$$

where the effective potential function reads as

$$\frac{V_{eff}}{E^2} = \frac{u^2}{r^2} A(r) - 1, \tag{14}$$

The unstable circular photon orbit of radius r_{ph} can be obtained from the conditions for the effective potential, given by $\frac{dV_{eff}}{dr}|_{r_{ph}} = 0$, and $\frac{d^2V_{eff}}{dr^2}|_{r_{ph}} < 0$, respectively. Thus the radius of the photon sphere r_{ph} is the largest real root of the equation

$$2A(r_{ph}) - r_{ph}A'(r_{ph}) = 0. \tag{15}$$

When the particle are coming at the closest distance $r = r_0$ to the central black hole, where $\frac{dr}{d\tau} = 0$, one can define the minimum impact parameter u_0 in terms of closest distance

r_0 [40] as

$$u_0 = \frac{r_0}{\sqrt{A(r_0)}} \tag{16}$$

The critical impact parameter for the unstable photon orbit u_{ph} is given by

$$u_{ph} = \frac{r_{ph}}{\sqrt{A(r_{ph})}} \tag{17}$$

The deflection angle in the strong field limit for a quantum-improved charged black hole spacetime, as a function of the closest approach distance r_0 , can be expressed as: [62, 63])

$$\alpha_D(r_0) = I(r_0) - \pi = 2 \int_{r_0}^{\infty} \frac{\sqrt{B(r)} dr}{\sqrt{C(r)} \sqrt{\frac{A(r)C(r)}{A(r_0)C(r_0)} - 1}} - \pi. \tag{18}$$

The strong deflection angle $\alpha_D(r_0)$ depends upon the relation between r_0 and r_{ph} and while $r_0 \approx r_{ph}$, it is increased. So, we consider a new variable z as:

$$z = 1 - \frac{r_0}{r}. \tag{19}$$

For, $r_0 \approx r_{ph}$, the strong deflection angle can be obtain as

$$\alpha_D(u) = -\bar{a} \log\left(\frac{u}{u_{ph}} - 1\right) + \bar{b} + \mathcal{O}((u - u_{ph}) \log(u - u_{ph})). \tag{20}$$

where the lensing coefficients \bar{a} and \bar{b} are formulated in [40].

The behavior of the strong deflection angle α_D for the quantum-improved charged black hole is depicted in Fig. 1 at the top-left corner panel, showing its variation with the parameter $\omega/4M^2$ for fixed $Q/2M$, as a function of the impact parameter u . Interestingly, this figure shows that the strong deflection angle decreases as the minimum impact parameter u increases, whereas the impact parameter u is close to the critical impact parameter u_{ph} . The deflection angle α_D approaches infinity as u tends to u_{ph} . Furthermore, from the top-middle panel in Fig. 1, it is seen that the deflection angle α_D with $u = u_{ph} + 0.0005$ grows when both the parameters $Q/2M$ and $\omega/4M^2$ increase simultaneously. This suggests that the quantum-improved charged black hole, with the presence of the parameters $Q/2M$ and $\omega/4M^2$, could greatly intensify the gravitational lensing effect. This result also indicates that the gravitational lensing effect due to the quantum-improved charged black hole is significantly enhanced compared to the other astrophysical black holes such as Schwarzschild, quantum-improved Schwarzschild, and Reissner-Nordstrom black holes. The parameter $\omega/4M^2$ may modify the trajectories of particles and photons, influencing the dynamics of matter and radiation in the vicinity of the black hole. Its introduction contributes to our understanding of how quantum effects manifest in the gravitational field of a charged black hole.

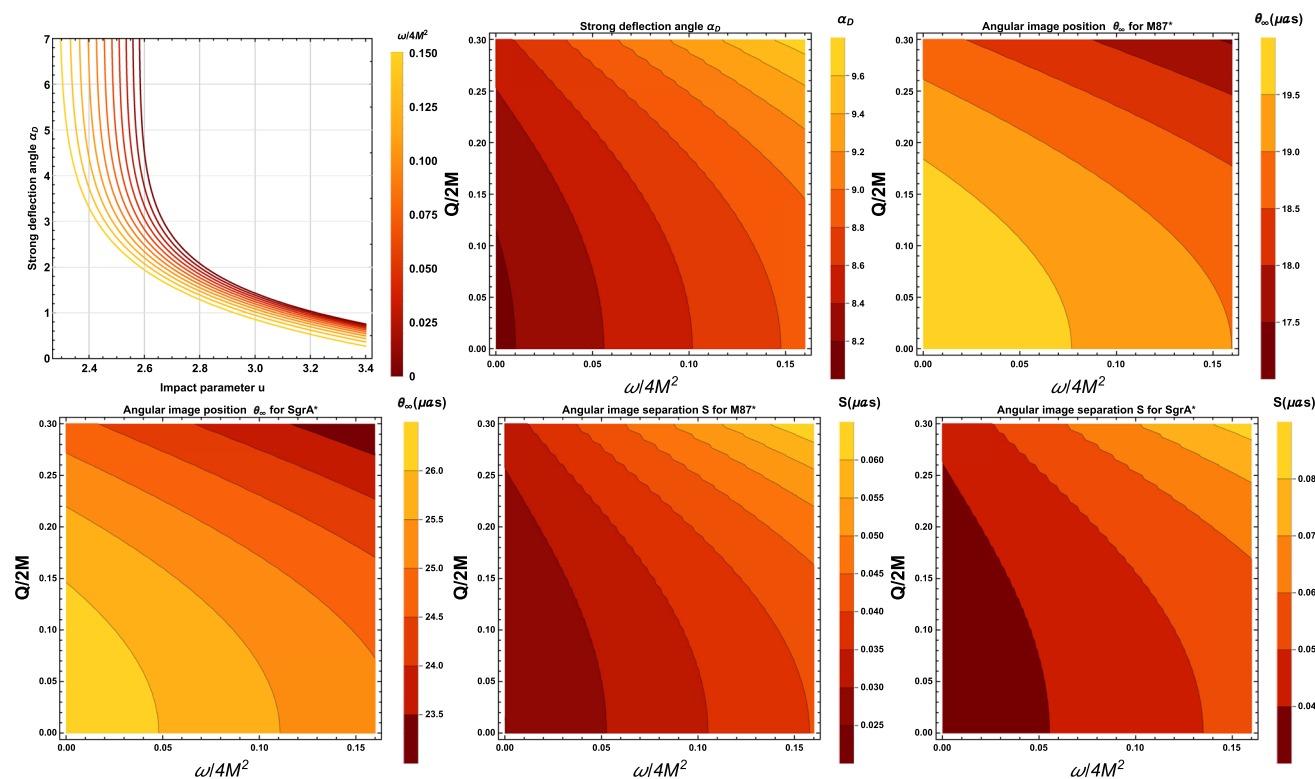


Fig. 1 Top left-corner panel, variation of the strong deflection angle for the quantum-improved charged black hole as a function of the impact parameter u . The deflection angle α_D approaches infinity as u tends to u_{ph} . The remaining figures illustrate the variations of the strong deflec-

tion angle α_D , angular image position θ_∞ (μas) of the relativistic image, and angular image separation S (μas) between two relativistic images for the supermassive black holes $M87^*$ and $SgrA^*$, respectively, and are presented as functions of the parameters $Q/2M$ and $\omega/4M^2$

Thus, the quantum-improved charged black hole with the presence of moving, fluid, matter and sound waves can be detected more easily and distinguished from the other astrophysical black holes such as Schwarzschild, quantum-improved Schwarzschild, and Reissner-Nordstrom black holes.

2.2 Lensing equation and observables

Next, we examine the various astrophysical consequences through strong gravitational lensing in the context of a quantum-improved charged black hole. In this regard, we consider a scenario where the observer and the source are situated significantly from the black hole (lens). Their alignment is nearly perfect along the optical axis, and they are placed in flat spacetime, with the curvature influencing the deflection angle primarily near the lens only [64]. Additionally, we assume that the source is positioned behind the black hole (lens). Consequently, we define the lens equation as [65,66]

$$\beta = \theta - \frac{D_{ls}}{D_{os}} \Delta\alpha_n \tag{21}$$

where $\Delta\alpha_n = \alpha_D(\theta) - 2n\pi$ represents the offset deflection angle, $\alpha_D(\theta)$ is the primary deflection angle, and n denotes the number of revolutions or loops that a photon ray makes around the black hole. The angles β and θ correspond to the angular separations between the black hole (lens) and the source or between the observer and the source, respectively. Here D_{ol}, D_{ls}, D_{os} are the observer-lens, lens-source, observer-source distance, respectively, such that $D_{os} = D_{ol} + D_{ls}$. Using Eqs. (20) and (21), the angular separation between the black hole (lens) and the n^{th} relativistic image can be expressed as

$$\theta_n = \theta_n^0 - \frac{u_{ph} e_n (\theta_n^0 - \beta) D_{os}}{\bar{a} D_{ol} D_{ls}}, \tag{22}$$

where

$$e_n = e^{\frac{\tilde{b} - 2n\pi}{\tilde{a}}},$$

and

$$\theta_n^0 = \frac{u_{ph}(1 + e_n)}{D_{ol}},$$

respectively. Here, θ_n^0 represents the angular position of the image when a photon completes a total of $2n\pi$ rotations

around the black hole (lens). In the context of strong gravitational lensing, where surface brightness is conserved, the magnification of the relativistic effect can be defined as the ratio of the solid angle covered by the n -th image to that covered by the source [67]. The magnification for the n -th relativistic image can be obtained as [40]

$$\mu_n = \left(\frac{\beta}{\theta} \frac{d\beta}{d\theta} \right)^{-1} \Big|_{\theta_n^0} = \frac{u_{ph}^2 (1 + e_n) e_n D_{os}}{\beta \bar{a} D_{ls} D_{ol}^2}. \tag{23}$$

The above equation strongly suggests that the first relativistic image holds the highest brightness level, and the magnification diminishes exponentially as 'n' increases. In other words, the brightness of this first image surpasses that of the subsequent relativistic images. Notably, Eq. (22) becomes unbounded when $\beta \rightarrow 0$, indicating that perfect alignment maximizes the possibility of detecting relativistic images. Here, we consider the case when the brightest image, i.e., the outermost image θ_1 is resolved as a single image, and the remaining inner images are packed together at θ_∞ ($\theta_n|_{n \rightarrow \infty} =: \theta_\infty$). With the help of the deflection angle given by Eq. (20), one can obtain strong lensing observables such as the angular position of the set of images θ_∞ , the angular separation between the outermost and innermost images, S and relative magnification r_{mag} between the outermost relativistic image and the inner relativistic images. These quantities can be defined as [40,68].

$$\theta_\infty = \frac{u_{ph}}{D_{ol}} \tag{24}$$

$$S = \theta_1 - \theta_\infty \approx \theta_\infty e^{\frac{(b-2\pi)}{\bar{a}}} \tag{25}$$

$$r_{mag} = \frac{\mu_1}{\sum_{n=2}^\infty \mu_n} \approx \frac{5\pi}{\bar{a} \log(10)} \tag{26}$$

If the strong lensing observables θ_∞, S , and r_{mag} are measured from the observations, the lensing coefficients \bar{a}, \bar{b} and the minimum impact parameter u_{ph} can be obtained easily by inverting the Eqs. (24), (25) and (26), respectively. Consequently, One can characterize the quantum-improved charged black hole from the other astrophysical black holes through observation. Considering the supermassive black holes $M87^*$ and $SgrA^*$ at the centers of nearby galaxies, we conducted numerical simulations to determine the observable quantities θ_∞, S , and r_{mag} for the quantum-improved charged black hole (see Table 1). According to [2], the mass and distance from Earth for $M87^*$ are approximately $6.5 \times 10^9 M_\odot$ and 16.8 Mpc, respectively. For $SgrA^*$, based on data from [69], the mass is approximately $4.28 \times 10^6 M_\odot$, and the distance is about 8.32 kpc. There is another important observable quantity, the Einstein ring, and it is extensively discussed in [70]. Through the simplification of Eq. (22) for $\beta = 0$, we obtain the angular radius of the n^{th} relativistic image as fol-

lows

$$\theta_n = \theta_n^0 \left(1 - \frac{u_{ph} e_n D_{os}}{\bar{a} D_{ls} D_{ol}} \right). \tag{27}$$

In the scenario where the black hole (lens) is positioned at a distance $D_{os} = 2D_{ol}$, the Einstein's ring becomes

$$\theta_n^E = \frac{u_{ph}(1 + e_n)}{D_{ol}}. \tag{28}$$

Time delay is one of the most important observable in the strong gravitational lensing effect. It results from the time difference between the formation of two relativistic images. The time difference appears when the photon travels in different paths around the black hole. The time travel for the photon paths for distinct relativistic images is not the same; hence, there is a time difference between the different relativistic images. If the time signals of two relativistic images are obtained from the observations, one can compute the time delay between the two signals [71]. The time taken by a photon to revolve around the black hole is given by [71]

$$\tilde{T} = \tilde{a} \log \left(\frac{u}{u_{ph}} - 1 \right) + \tilde{b} + \mathcal{O}(u - u_{ph}). \tag{29}$$

With the help of the above Eq. (29), one can compute the time difference between two relativistic images. For spherically static symmetric black hole spacetime, the time delay between two relativistic images, when the relativistic images are on the same side of the black hole, are obtained as

$$\Delta T_{2,1} = 2\pi u_{ph} = 2\pi D_{ol} \theta_\infty \tag{30}$$

Using Eq. (30), if one can measure the time delay with high accuracy and the critical impact parameter with negligible error, then one can determine the quantum nature of black holes with that specific level of accuracy.

The strong lensing observables angular image position of the innermost images $\theta_\infty(\mu as)$ of the relativistic image, angular image separation $S(\mu as)$ between two relativistic images, and relative magnification of the relativistic images r_{mag} for the supermassive black holes $M87^*$ and $SgrA^*$, respectively, are presented as functions of the parameters $Q/2M$ and $\omega/4M^2$ in Figs. 1 and 2 and also in Table 1. In these figures and this table, it is observed that the angular image position $\theta_\infty(\mu as)$ and relative magnification of r_{mag} of the images decreases while the angular image separation $S(\mu as)$ between two relativistic images increases when both the parameters $Q/2M$ and $\omega/4M^2$ increase simultaneously. Furthermore, considering the same mass and distance of the black hole, it is observed in our estimation that the angular position of the innermost images, θ_∞ for quantum-improved charged black hole ($Q/2M = 0.1, \omega/4M^2 = 0.02$) is greater than that in the cases of quantum-improved Schwarzschild ($Q/2M = 0, \omega/4M^2 = 0.1$) and Reissner-Nordström ($Q/2M = 0.2, \omega/4M^2 = 0$) black holes

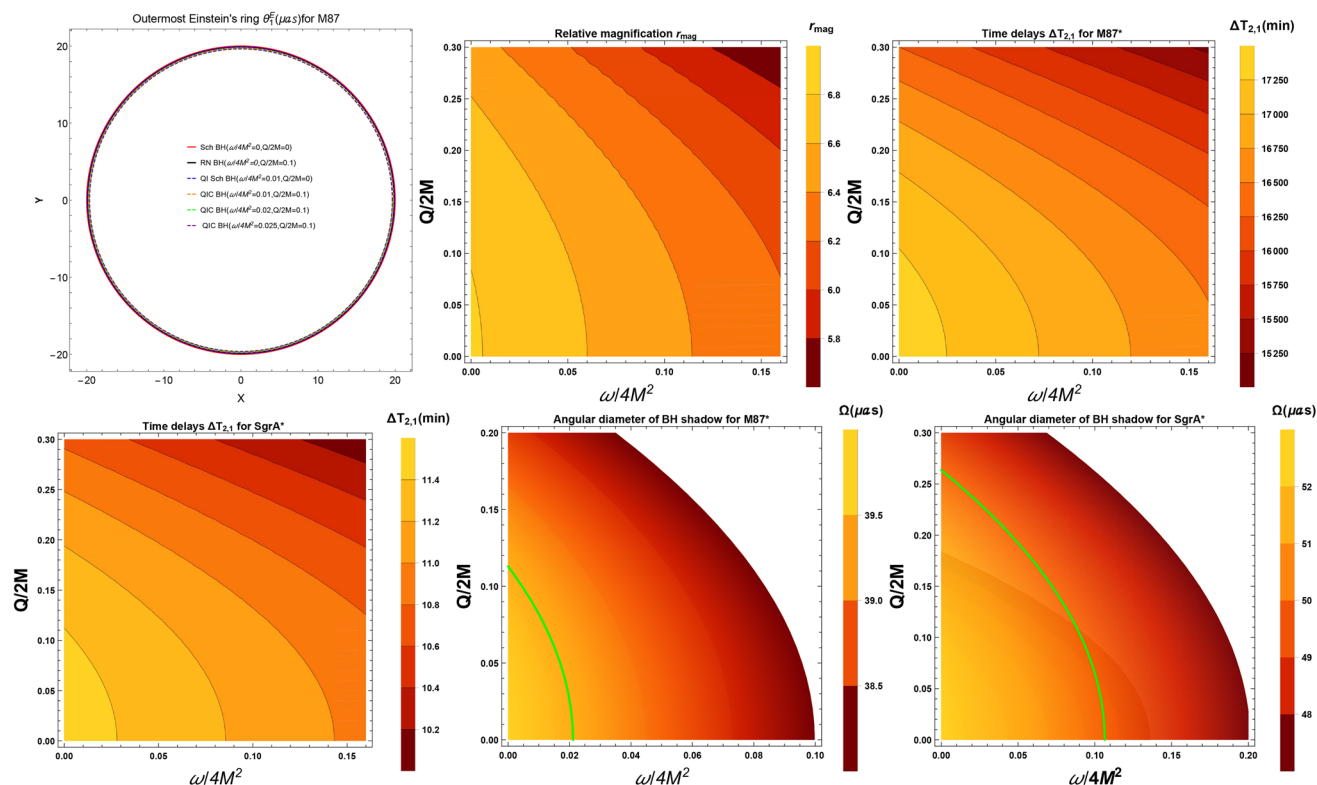


Fig. 2 Top left-corner panel, variation of the outermost Einstein’s ring for $M87^*$ in the context of quantum-improved charged and compared to the cases of Schwarzschild, quantum-improved Schwarzschild, and Reissner-Nordström black holes. The red, black, and blue curves correspond to the cases of Schwarzschild, Reissner–Nordström, and quantum-improved Schwarzschild black holes, respectively. The remaining figures illustrate the variations of the relative magnification r_{mag} of the relativistic image, time-delay $\Delta T_{2,1}$ (minutes) between two relativistic images, and the angular diameter of the black hole shadow $\Omega (= 2\theta_\infty)\mu as$ for the supermassive black holes $M87^*$ and $Sgr A^*$,

respectively, and are presented as functions of the parameters $Q/2M$ and $\omega/4M^2$. In the lower middle panel, the green solid curve corresponds to $\Omega = 39.4\mu as$ for $M87^*$, and this value falls within the 1σ region of the measured angular diameter, $\Omega = 42 \pm 3\mu as$, in the parameter space $(\omega/4M^2, Q/2M)$ for $M87^*$. In the lower right corner panel, the green solid curve corresponds to $\Omega = 49.9\mu as$ for $Sgr A^*$, and this value also falls within the 1σ region of the measured angular diameter, $\Omega = 51.8 \pm 2.3\mu as$, in the parameter space $(\omega/4M^2, Q/2M)$ for $Sgr A^*$

and smaller than the case of Schwarzschild ($Q/2M = 0, \omega/4M^2 = 0.1$) black holes. Also, the quantum-improved charged black hole ($Q/2M = 0.1, \omega/4M^2 = 0.02$) has smaller image separation $S \sim 0.028\mu as$. It means that the outermost images for the quantum-improved charged black hole are closest to the innermost images and can be separated from the other black hole images. In addition, if the outermost brightest relativistic image can be resolved, we may distinguish the quantum-improved charged black hole from a Schwarzschild, quantum-improved Schwarzschild, or Reissner-Nordström black hole using the new current technology. Although detecting the images is challenging due to the small deviation in image separation (~ 0.01), we must await EHT observations. Astrophysical consequences such as outermost Einstein’s rings θ_1^E for $M87^*$, time delay $\Delta T_{2,1}$ between the second and first relativistic images, and angular diameter of black hole shadow Ω are depicted in Fig. 2. It is observed that the Einstein ring θ_1^E for the

quantum-improved charged black hole is greater than the cases of Schwarzschild, quantum-improved Schwarzschild and Reissner-Nordström black holes. These observables influenced by the quantum nature introduced by ω in the context of the charged black hole impact the gravitational lensing features around the black hole. The parameter ω representing quantum corrections significantly influences the gravitational lensing characteristics and the overall geometry around the black hole. In Fig. 2 and this Table 1, it is also observed that time delay $\Delta T_{2,1}$ between the second and first relativistic images in the context of both $M87^*$ and $Sgr A^*$ decreases when both the parameters $Q/2M$ and $\omega/4M^2$ increase simultaneously. Moreover, considering the same mass and distance of the black hole ($M87^*$), it is observed in our estimation that time delay $\Delta T_{2,1}$ quantum-improved charged black hole ($Q/2M = 0.1, \omega/4M^2 = 0.02$) is ~ 17102.3 minutes, greater than that in the cases of quantum-improved Schwarzschild ($Q/2M = 0, \omega/4M^2 =$

0.1) and Reissner-Nordström ($Q/2M = 0.2, \omega/4M^2 = 0$) black holes and smaller than the case of Schwarzschild ($Q/2M = 0, \omega/4M^2 = 0.1$) black holes. It suggests that if the first and second relativistic images can be separated through observation, the time delay between them might offer an excellent opportunity to distinguish the quantum-improved charged black hole from a quantum-improved Schwarzschild, Reissner-Nordström, or Schwarzschild black hole. These observational studies of gravitational lensing effects provide valuable insights into the quantum nature of black holes in astrophysical contexts.

In the lower middle panel in Fig. 2, the green solid curve corresponds to $\Omega = 39.4\mu as$ for $M87^*$, and this value falls within the 1σ region of the measured angular diameter, $\Omega = 42 \pm 3\mu as$, in the parameter space ($\omega/4M^2, Q/2M$) for $M87^*$. In the lower right corner panel in Fig. 2, the green solid curve corresponds to $\Omega = 49.9\mu as$ for $SgrA^*$, and this value also falls within the 1σ region of the measured angular diameter, $\Omega = 51.8 \pm 2.3\mu as$, in the parameter space ($\omega/4M^2, Q/2M$) for $SgrA^*$. Our observations indicate constrained parameter spaces for the black hole: $0 \leq \omega/4M^2 \leq 0.0216$ and $0 \leq Q/2M \leq 0.114$ for $M87^*$; and $0 \leq \omega/4M^2 \leq 0.1072$ and $0 \leq Q/2M \leq 0.266$ for $SgrA^*$. These additional parameters, $\omega/4M^2$ and $Q/2M$, characterize the quantum-improved charged black holes similar to the supermassive black holes $M87^*$ and $SgrA^*$. Our results suggest that the quantum-improved charged black

hole complies with the EHT constraint, indicating its potential detectability and distinguishability from other astrophysical black holes in future observations.

3 Oscillations of massive particles around quantum-improved charged black hole

Quantum-improved charged black holes are theoretically constructed models that take into account the effects of quantum mechanics on black hole properties. These effects can lead to modifications of the black hole’s spacetime geometry near its event horizon, which can influence the dynamics of matter and radiation in the black hole’s vicinity. The epicyclic frequencies associated with the QPOs of test particles around the effective region of the ISCO radius are covered in this section. One may find a comprehensive formulation and background of these frequencies in [72]. The creation and behavior of QPOs in black hole systems may be affected by these quantum effects, according to certain theories. For instance, specific oscillation modes in the accretion disk or jet may be stimulated by the modified spacetime geometry close to a quantum-improved charged black hole, resulting in the observed QPOs. The QPOs that stellar-mass black hole binaries show in their X-ray flux light curves have long been recognized, and this phenomenon is thought to be one of the most useful ways to test strong gravity models. These oscilla-

Table 1 Estimate various strong lensing observables for Schwarzschild, RN, quantum improved and quantum improved charged BHs in the context of supermassive BHs $M87^*$ and $SgrA^*$ while considering different values of the parameters Q and ω

Parameters		$M87^*$			$SgrA^*$			SMBHs
Q	ω	$\theta_\infty (\mu as)$	$S (\mu as)$	$\Delta T_{2,1} (\text{min})$	$\theta_\infty (\mu as)$	$S (\mu as)$	$\Delta T_{2,1} (\text{min})$	r_{mag}
0	0	19.9632	0.024984	17378.8	26.3826	0.0330177	11.4973	6.82188
0	0.1	18.9984	0.0402126	16538.9	25.1075	0.0531433	10.9417	6.23087
0.2	0	19.4132	0.02773324	16900	25.6557	0.0366511	11.1805	6.68985
	0.02	19.6456	0.02794	17102.3	25.9628	0.0369244	11.3144	6.68392
	0.04	19.4559	0.0306376	16937.2	25.7122	0.0404894	11.2052	6.57028
0.1	0.06	19.2596	0.0337776	16766.3	25.4527	0.0446391	11.0921	6.44905
	0.08	19.0557	0.0374694	16588.8	25.1832	0.049518	10.9747	6.31903
	0.1	18.8434	0.0418599	16404	24.9027	0.0553203	10.8524	6.17865
0.2	0.02	19.2183	0.0305153	16730.3	25.3981	0.0403277	11.0683	6.57202
	0.04	19.0161	0.0337756	16554.3	25.1309	0.0446364	10.9519	6.44589
	0.06	18.8058	0.0376387	16371.3	24.853	0.0497417	10.8308	6.31004
	0.08	18.5863	0.0422749	16180.2	24.5629	0.0558688	10.7043	6.16267
0.25	0.1	18.3563	0.0479233	15979.9	24.2589	0.0633335	10.5718	6.00137
	0.02	18.8815	0.0328935	16437.2	24.9531	0.0434707	10.8744	6.47663
	0.04	18.6683	0.0367223	16251.5	24.6712	0.0485306	10.7516	6.3388
	0.06	18.4455	0.041335	16057.5	24.3768	0.0546267	10.6232	6.18899
0.1	0.08	18.2116	0.0469808	15854	24.0678	0.0620879	10.4886	6.02462
	0.1	17.965	0.0540232	15639.3	23.7418	0.0713948	10.3465	5.84216

tions appear near the black hole and exhibit frequencies that are inversely related to the mass of the black hole. We can precisely measure the frequencies of QPOs using the current state of observational data, giving us information about the centre and its surroundings of compact objects. There are three types of fundamental frequencies. One of them is the orbital frequency or Keplerian frequency, i.e., $v_\phi = W_\phi/2\pi$ second one is the radial epicyclic frequency $v_r = W_r/2\pi$, which is the radial oscillation frequency in the vicinity of the mean orbit. The last one is known as vertical epicyclic frequency, i.e., $v_\theta = W_\theta/2\pi$. The mathematical formulas within the scope of the quantum-improved charged black holes are defined as follows:

$$W_\phi = \frac{d\phi}{dt} = \frac{\pm \left(\sqrt{\left(\frac{\partial g_{t\phi}}{\partial r} \right)^2 - \frac{\partial g_{tt}}{\partial r} \frac{\partial g_{\phi\phi}}{\partial r}} - \left(\frac{\partial g_{t\phi}}{\partial r} \right) \right)}{\frac{\partial g_{\phi\phi}}{\partial r}}, \tag{31}$$

$$W_r^2 = -\frac{\partial^2 V_{eff}}{\partial r^2} \left(\frac{1}{2t^2 g_{rr}} \right), \tag{32}$$

$$W_\theta^2 = -\frac{\partial^2 V_{eff}}{\partial \theta^2} \left(\frac{1}{2t^2 g_{\theta\theta}} \right). \tag{33}$$

As we are working with the non-rotation version of the black hole solution, we will analyze only two cases, like v_ϕ and v_r . The vertical epicyclic frequency v_θ should be considered equal to v_ϕ in the current study. All the fundamental frequencies of the massive particles around the quantum-improved charged black hole are calculated as:

$$v_r = \frac{\sqrt{v_{1r}}}{2\pi}, \tag{34}$$

$$v_\phi = v_\theta = \frac{\sqrt{-\frac{Gr(GM\omega - Mr^2 + Q^2r)}{(G\omega + r^2)^2}}}{2\pi r}, \tag{35}$$

where

$$\begin{aligned} & -\frac{-2Mr + Q^2 + r^2 + \omega}{(r^2 + \omega)^4 (-Mr(3r^2 + \omega) + Q^2(2r^2 + \omega) + (r^2 + \omega)^2)^3} \left[-r(r^2 + \omega)^2 (-2Mr + Q^2 + r^2 + \omega) (Q^2 \right. \\ & \times (M^2(18r^7 + 25r^5\omega + 36r^3\omega^2 - 3r\omega^3) + M(5r^8 - 18r^6\omega - 45r^4\omega^2 - 32r^2\omega^3 + 6\omega^4) - 6r\omega(r^2 - \omega) \\ & \times (r^2 + \omega)^2) + M(M^2(-9r^8 - 9r^6\omega - 15r^4\omega^2 + r^2\omega^3) + Mr\omega(15r^6 + 35r^4\omega + 33r^2\omega^2 - 3\omega^3) + 3\omega \\ & \times (r^2 + \omega)^2(r^4 - 6r^2\omega + \omega^2)) - Q^4(M(12r^6 + 15r^4\omega + 20r^2\omega^2 - 3\omega^3) + 2(3r^7 + r^5\omega - 6r^3\omega^2 - 6r\omega^3)) \\ & \left. + Q^6(4r^5 + 6r^3\omega + 6r\omega^2) \right) + (Q^2(3r^2 - \omega) - 2Mr(r^2 - 3\omega))(-Mr(3r^2 + \omega) + Q^2(2r^2 + \omega) \\ & + (r^2 + \omega)^2)^2 (M(r^5 - r^3(\omega + 3) - r\omega) + Q^2(-r^4 + 2r^2 + \omega) + (r^2 + \omega)^2) + 2r^2(r^2 + \omega)^2 \\ & \times (M(\omega - r^2) + Q^2r)(-Mr(3r^2 + \omega) + Q^2(2r^2 + \omega) + (r^2 + \omega)^2) (M\omega(-2Mr + 3Q^2 + 3\omega) \\ & \left. \times +r(Q^2(4\omega - 9Mr) + 6Mr(Mr - \omega) + 4Q^4) - Mr^4) x \right] \end{aligned}$$

The above-calculated frequencies depend upon the spacetime involved parameters ω and charged Q . One can see the graphical analysis of these frequencies in Fig. 3 for different values

of involved parameters. The radial epicyclic frequency goes away from the effective region of the ISCO radius for the small values of parameter ω and gets closer to the effective region of the ISCO radius for the larger values of parameter ω . Similarly, the larger values of charge parameter Q lead to very close to the ISCO region, and due to the small values of Q , the effect of radial epicyclic frequency is decreasing. The different values of ω and Q have no impact on orbital frequency or Keplerian frequency.

4 Tested high frequency QPOs models

According to the hot spot models, radiating spots in thin accretion discs have geodesic paths that are almost circular. The resonance of axisymmetric oscillation modes of accretion discs is taken into consideration by the ER model [73]. The orbital and epicyclic frequencies of the circular geodesic motion are connected to the disc oscillation frequencies. It is assumed that the oscillating torus (or circle) in the ER model with axisymmetric oscillatory modes at frequency v_ϕ and v_r radiates uniformly. The nodal frequency associated with the radiating torus's orbiting frequency v_ϕ can be introduced when there is a significant enough inhomogeneity on the torus. In the current analysis, we have considered four ER models, say ER0 ($v_U = v_\phi$ and $v_L = v_\phi - v_r$), ER1 ($v_U = v_\phi$ and $v_L = v_\phi - v_r$), ER3 ($v_U = v_\phi + v_r$ and $v_L = v_\phi$), and ER4 ($v_U = v_\phi + v_r$ and $v_L = v_\phi - v_r$) [74] due the choice of no-rotating black hole geometry. The graphical behavior for ER0, ER1, ER3, and ER4 is provided in Figs. 3, 4, 5 and 6. From these figures, a satisfying behavior within the scope of upper and lower frequencies is perceived.

The orbital frequency, $v_U = v_\phi$, is associated with the upper of the twin frequencies in the conventional RP model

[75], while the periastron precession frequency, $v_L = v_\phi - v_r$, is associated with the lower one. We choose the RPO model, presented in [76], where $v_U = v_\phi$ and $v_L = v_\phi - v_r$,

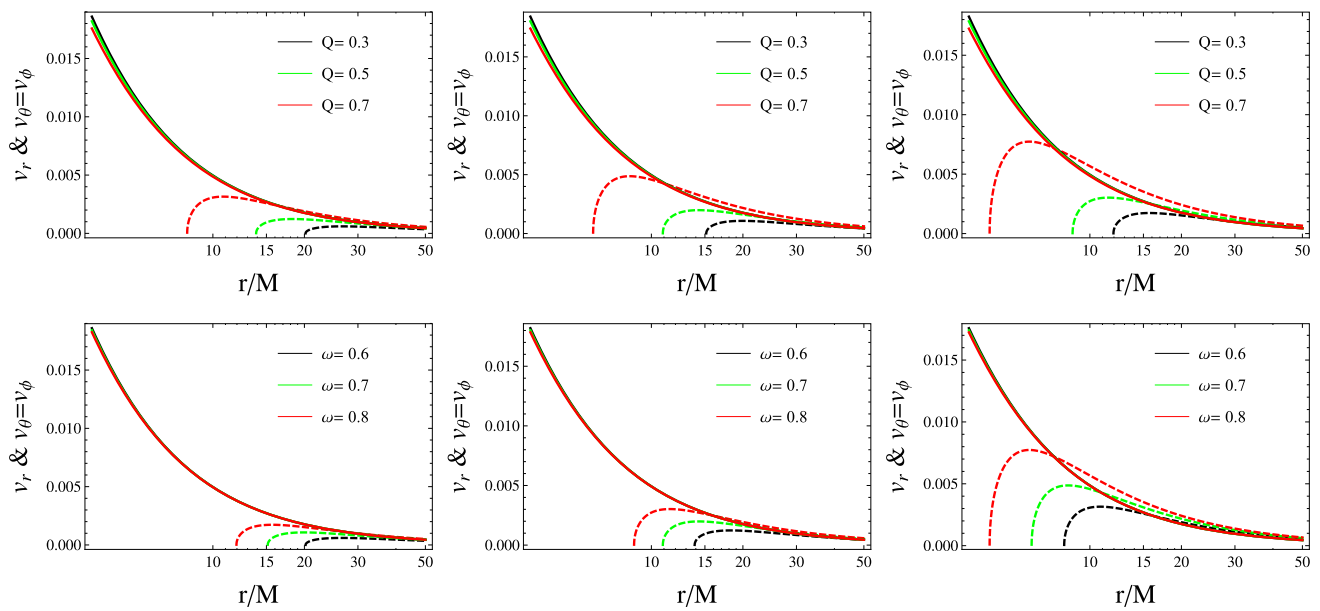


Fig. 3 Radial and tangential frequencies v_r & $v_\theta = v_\phi$ around a quantum-improved charged black hole with radial frequency (dotted lines) and orbital frequency (solid lines)

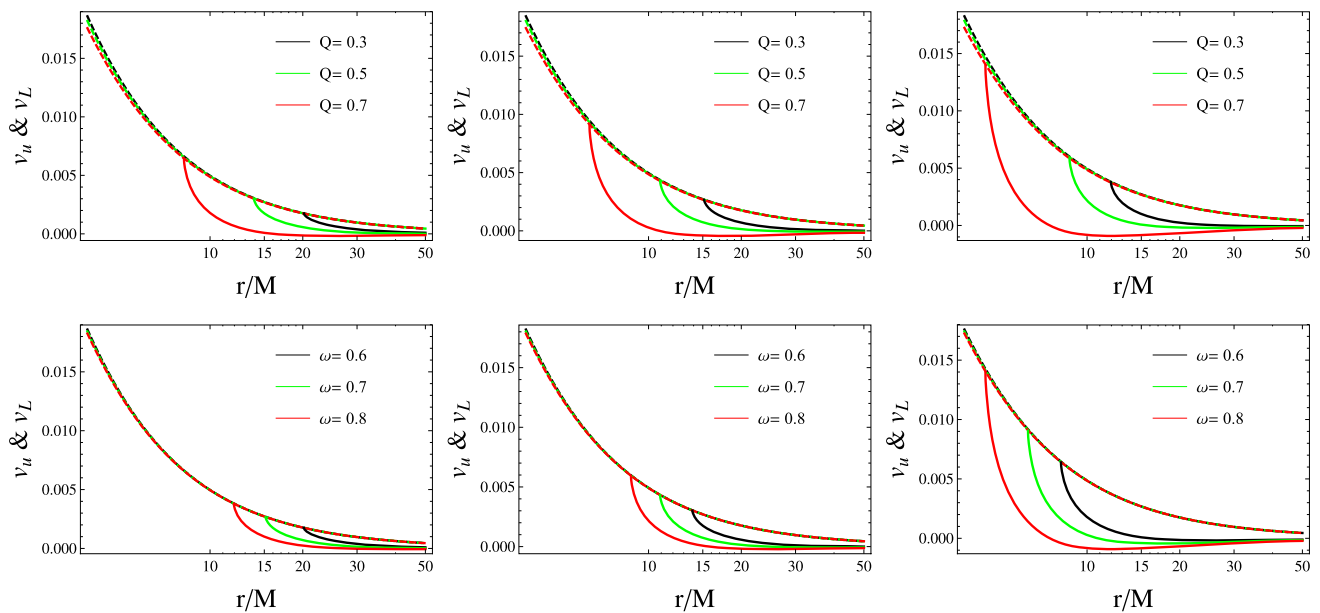


Fig. 4 Shows the ER1 ($v_U = v_\phi$ (dotted lines) and $v_L = v_\phi - v_r$ (solid lines)) high-frequency QPOs model around quantum-improved charged black hole

and the RP1 “total precession model,” introduced in [77], should be same like RP0 in the current analysis. The frequencies v_U and v_L predicted by the RP0 and RP1 models are similar to those of the RP model. The graphical behavior for RP0 ($v_U = v_\phi$ and $v_L = v_\phi - v_r$) is provided in Fig. 7. Figure 7 confirms the upper and lower required behaviour. For the WD model, we have to introduce the vertical oscillatory frequency v_ϕ by assuming vertical axisymmetric oscillations of the thin disc. The WD oscillation model of twin

High-Frequency QPOs assumes non-axisymmetric oscillatory modes of a thin disc [78]. The graphical behavior for WD ($v_U = 2v_\phi - v_r$ and $v_L = 2(v_\phi - v_r)$) is provided in Fig. 7. The upper and lower required behavior can be confirmed from Fig. 8. We examine the frequencies in the background of high-frequency QPO models that have been altered by particle motion around a charged black hole that has undergone quantum improvement.

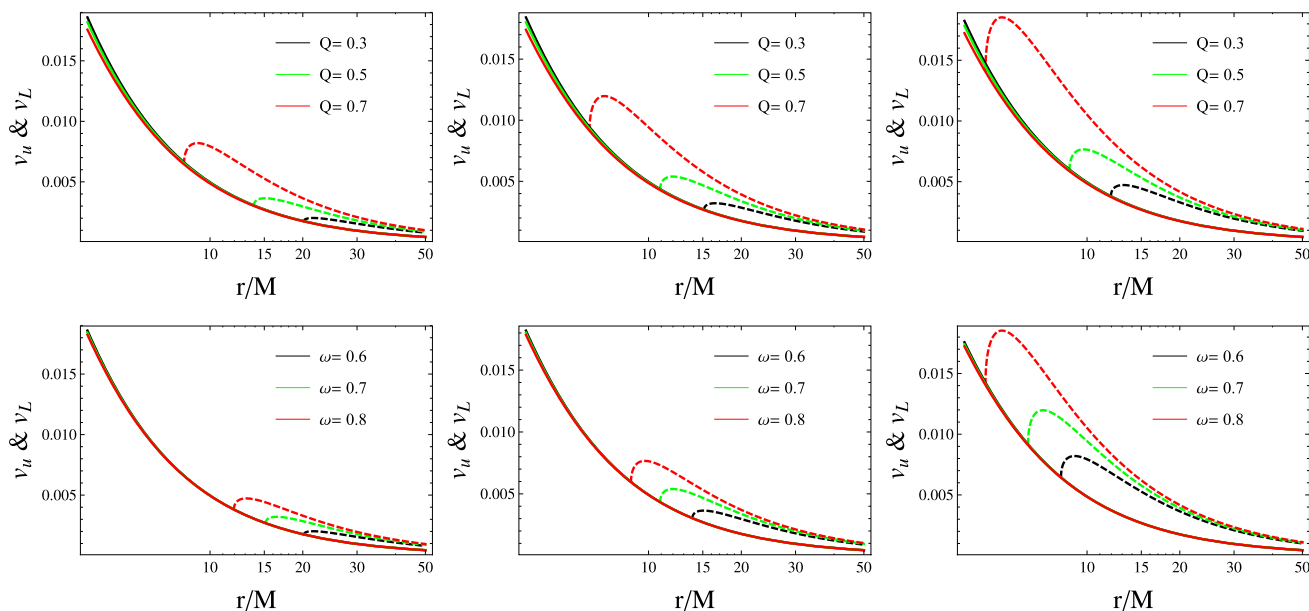


Fig. 5 Shows the ER3 ($v_U = v_\phi + v_r$ (dotted lines) and $v_L = v_\phi$ (solid lines)) high-frequency QPOs model around quantum-improved charged black hole

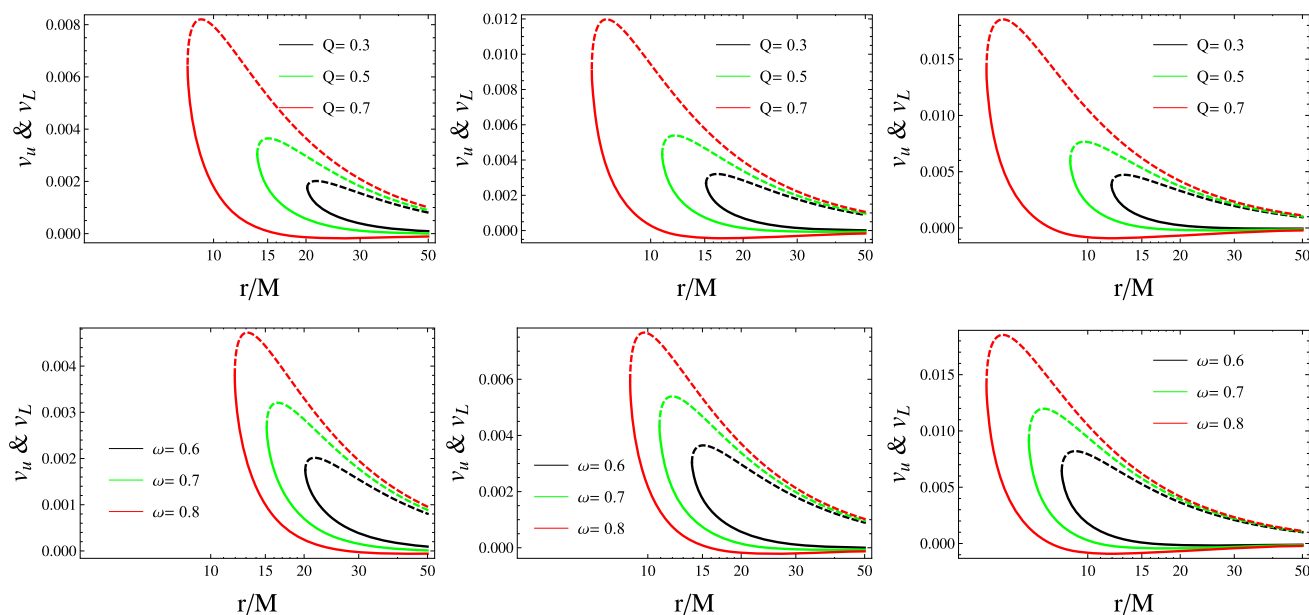


Fig. 6 Shows the ER4 ($v_U = v_\phi + v_r$ (dotted lines) and $v_L = v_\phi - v_r$ (solid lines)) high-frequency QPOs model around quantum-improved charged black hole

5 Concluding remarks

In this research work, we have discussed the strong gravitational lensing phenomena and QOPs by the quantum-improved charged black hole. This study explored the impact of the quantum parameter ω and the geometric charge Q on Schwarzschild black holes. Gravitational lensing in the strong field limit provides a powerful tool to identify the nature of the black holes in the quantum theory of grav-

ity or modified theory of gravity. For this purpose, we first obtain the deflection angle in the strong field limit. It is observed that the deflection angle α_D grows when both the parameters $Q/2M$ and $\omega/4M^2$ increase simultaneously. This suggests that the quantum-improved charged black hole, with the presence of the parameters $Q/2M$ and $\omega/4M^2$ could greatly intensify the gravitational lensing effect. The results imply that studying gravitational lensing by quantum-improved charged black holes may provide insights into the

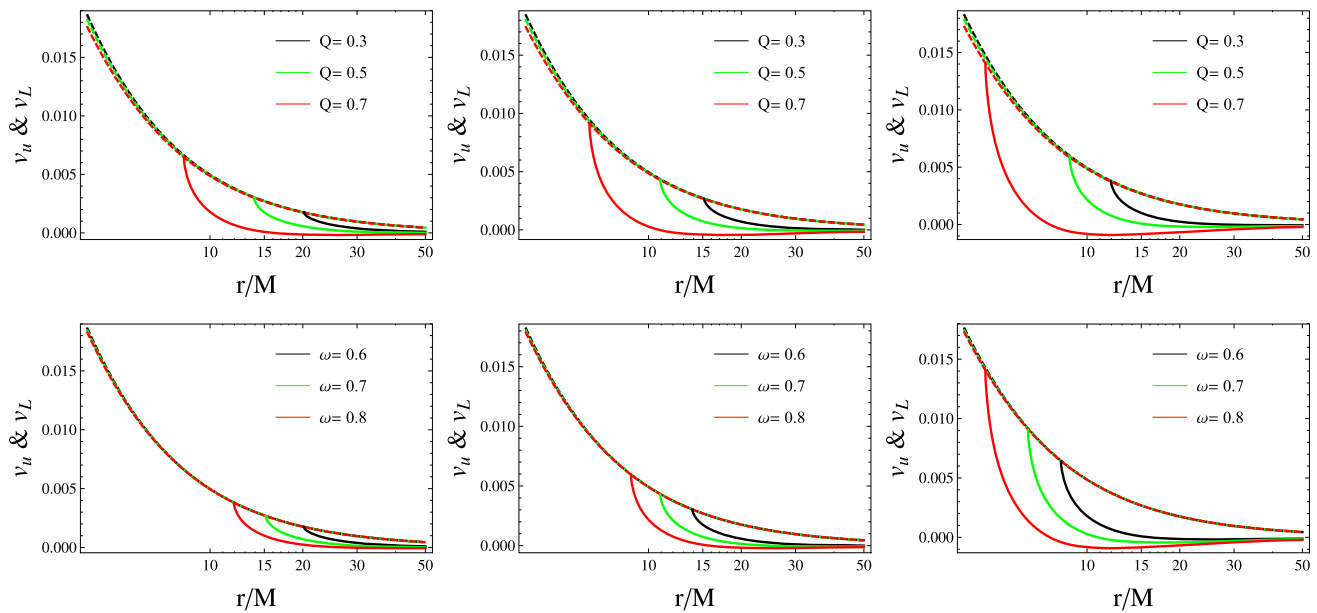


Fig. 7 Shows the RP0 ($v_U = v_\phi$ (dotted lines) and $v_L = v_\phi - v_r$ (solid lines)) high-frequency QPOs model around quantum-improved charged black hole

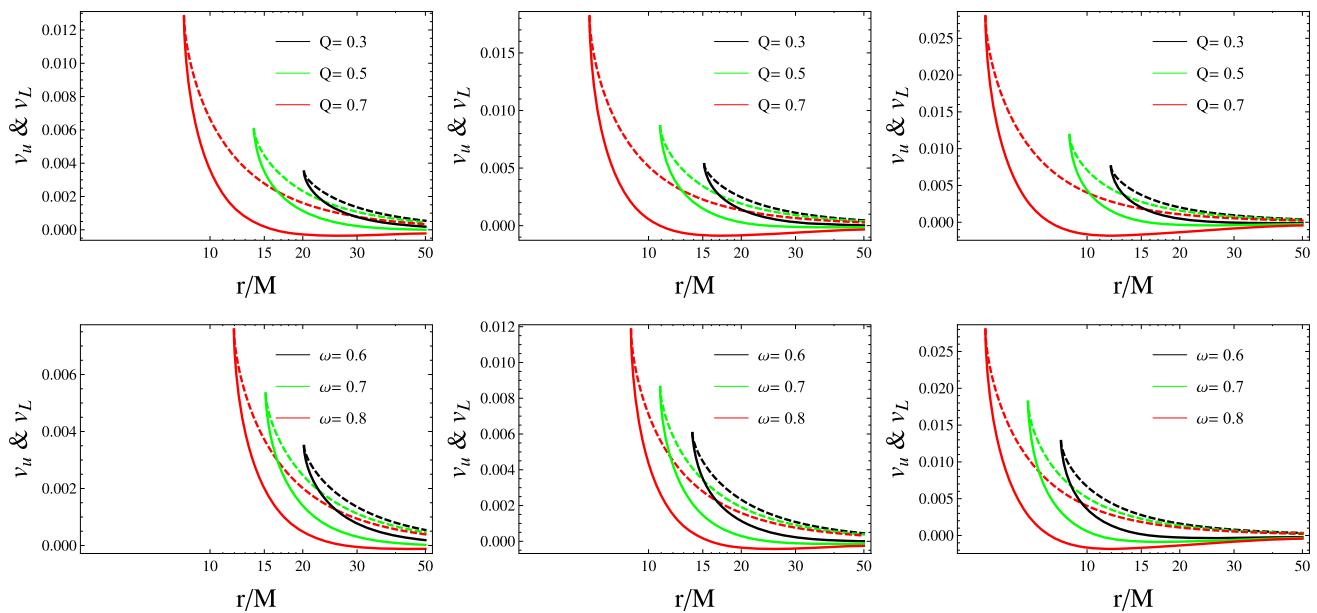


Fig. 8 Shows the WD ($v_U = 2v_\phi - v_r$ (dotted lines) and $v_L = 2(v_\phi - v_r)$ (solid lines)) high-frequency QPOs model around quantum-improved charged black hole

interplay between quantum effects and gravity. This study could contribute to our understanding of quantum gravity in the strong gravitational field regime near the charged black holes. We also study the various astrophysical implications by considering the examples of supermassive black holes *M87** and *SgrA** through strong gravitational lensing and observe that the quantum-improved charged black hole could be quantitatively distinguished from the quantum-improved Schwarzschild, Reissner-Nordström, and Schwarzschild black

holes. The quantitative distinctions in the gravitational lensing effect between the quantum-improved charged black hole and ordinary black holes (such as Schwarzschild, Reissner-Nordström) indicate that astrophysical observations have the potential to differentiate between these different types of black holes based on their quantum characteristics. The observational findings, elucidating various astrophysical consequences through gravitational lensing effects, offer valuable insights into the quantum nature of

black holes in the astrophysical contexts. Thus, Quantum corrections to classical black hole solutions may introduce novel phenomena detectable through astrophysical observations, specifically via strong gravitational lensing phenomena. By considering the EHT constraints on $M87^*$ and $Sgr A^*$ within the 1σ region and setting bounds on the parameters $Q/2M$ and $\omega/4M^2$, our analysis indicates that the quantum-improved charged black hole is consistent with the EHT results within a finite parameter space. Importantly, this suggests that quantum-improved charged black holes cannot be ruled out as strong candidates for astrophysical black holes. We have examined the radial profiles of the radial and orbital frequencies as well as the fundamental frequencies of test particles around quantum-improved charged black holes. We have studied the positioning of resonant radii in the background of quantum-improved charged black holes for high-frequency QOPs models: warped disc models, relativistic precession and its types, and epicyclic resonance and its variants. It is necessary to mention that the above and lower behavior of these relativistic models has been satisfied in the current analysis. It has also been observed that the particles moving around quantum-improved charged black holes have high frequencies.

Acknowledgements N.U.M would like to thank CSIR, Govt. of India for providing Senior Research Fellowship (No. 08/003(0141))/2020-EMR-I). The author S. K. Maurya acknowledges the authority of University of Nizwa for their continuous support and encouragement to carry out this research work. G. Mustafa is very thankful to Prof. Gao Xianlong from the Department of Physics, Zhejiang Normal University, for his kind support and help during this research. Further, G. Mustafa acknowledges grant No. ZC304022919 to support his Postdoctoral Fellowship at Zhejiang Normal University, PR China.

Data availability statement This manuscript has no associated data or the data will not be deposited. [Authors' comment: There is no observational data pertaining to this study have been investigated. This work has already included a comprehensive analysis and the corresponding calculations.]

Open Access This article is licensed under a Creative Commons Attribution 4.0 International License, which permits use, sharing, adaptation, distribution and reproduction in any medium or format, as long as you give appropriate credit to the original author(s) and the source, provide a link to the Creative Commons licence, and indicate if changes were made. The images or other third party material in this article are included in the article's Creative Commons licence, unless indicated otherwise in a credit line to the material. If material is not included in the article's Creative Commons licence and your intended use is not permitted by statutory regulation or exceeds the permitted use, you will need to obtain permission directly from the copyright holder. To view a copy of this licence, visit <http://creativecommons.org/licenses/by/4.0/>.
Funded by SCOAP³.

References

1. B.P. Abbott et al., Properties of the Binary Black Hole Merger GW150914. *Phys. Rev. Lett.* **116**(24), 241102 (2016). <https://doi.org/10.1103/PhysRevLett.116.241102>
2. K. Akiyama et al., First M87 Event Horizon Telescope Results. I. The Shadow of the Supermassive Black Hole. *Astrophys. J. Lett.* **875**, L1 (2019). <https://doi.org/10.3847/2041-8213/ab0ec7>
3. J. Kumar, S.U. Islam, S.G. Ghosh, Strong gravitational lensing by loop quantum gravity motivated rotating black holes and EHT observations. *Eur. Phys. J. C* **83**(11), 1014 (2023). <https://doi.org/10.1140/epjc/s10052-023-12205-3>. arXiv:2305.04336
4. A. Anjum, M. Afrin, S.G. Ghosh, Investigating effects of dark matter on photon orbits and black hole shadows. *Phys. Dark Univ.* **40**, 101195 (2023). <https://doi.org/10.1016/j.dark.2023.101195>. arXiv:2301.06373,
5. L.-M. Cao, L.-B. Wu, Y. Zhao, Y.-S. Zhou, Quasinormal modes of tensor perturbations of Kaluza-Klein black holes in Einstein-Gauss-Bonnet gravity. *Phys. Rev. D* **108**(12), 124023 (2023). <https://doi.org/10.1103/PhysRevD.108.124023>
6. M. Bojowald, Loop quantum cosmology. *Living Rev. Rel.* **8**, 11 (2005). <https://doi.org/10.12942/lrr-2005-11>. arXiv:gr-qc/0601085
7. C. Menchon, G.J. Olmo, D. Rubiera-Garcia, Nonsingular black holes, wormholes, and de Sitter cores from anisotropic fluids. *Phys. Rev. D* **96**(10), 104028 (2017). <https://doi.org/10.1103/PhysRevD.96.104028>. arXiv:1709.09592
8. C. Bejarano, G.J. Olmo, D. Rubiera-Garcia, What is a singular black hole beyond General Relativity? *Phys. Rev. D* **95**(6), 064043 (2017). <https://doi.org/10.1103/PhysRevD.95.064043>. arXiv:1702.01292
9. V.P. Frolov, G.A. Vilkovisky, Spherically Symmetric Collapse in Quantum Gravity. *Phys. Lett. B* **106**, 307–313 (1981). [https://doi.org/10.1016/0370-2693\(81\)90542-6](https://doi.org/10.1016/0370-2693(81)90542-6)
10. P.O. Mazur, E. Mottola, Gravitational vacuum condensate stars. *Proc. Nat. Acad. Sci.* **101**, 9545–9550 (2004). <https://doi.org/10.1073/pnas.0402717101>. arXiv:gr-qc/0407075
11. M. Visser, D.L. Wiltshire, Stable gravastars: An Alternative to black holes? *Class. Quant. Grav.* **21**, 1135–1152 (2004). <https://doi.org/10.1088/0264-9381/21/4/027>. arXiv:gr-qc/0310107
12. S.D. Mathur, The Information paradox: A Pedagogical introduction. *Class. Quant. Grav.* **26**, 224001 (2009). <https://doi.org/10.1088/0264-9381/26/22/224001>. arXiv:0909.1038,
13. S.D. Mathur, D. Turton, Comments on black holes i: the possibility of complementarity. *J. High Energy Phys.* **2014**(1), 1–32 (2014)
14. V. Cardoso, E. Franzin, P. Pani, Is the gravitational-wave ringdown a probe of the event horizon?, *Phys. Rev. Lett.* **116**(17), 171101 (2016). [Erratum: *Phys. Rev. Lett.* **117**, 089902 (2016)]. <https://doi.org/10.1103/PhysRevLett.116.171101>. arXiv:1602.07309
15. S.M. Du, Y. Chen, Searching for near-horizon quantum structures in the binary black-hole stochastic gravitational-wave background. *Phys. Rev. Lett.* **121**(5), 051105 (2018). <https://doi.org/10.1103/PhysRevLett.121.051105>. arXiv:1803.10947
16. S.B. Giddings, Gravitational wave tests of quantum modifications to black hole structure - with post-GW150914 update. *Class. Quant. Grav.* **33**(23), 235010 (2016). <https://doi.org/10.1088/0264-9381/33/23/235010>. arXiv:1602.03622
17. S.D. Mathur, The Fuzzball proposal for black holes: An Elementary review. *Fortsch. Phys.* **53**, 793–827 (2005). <https://doi.org/10.1002/prop.200410203>. arXiv:hep-th/0502050
18. S.L. Liebling, C. Palenzuela, Dynamical boson stars. *Living Rev. Rel.* **26**(1), 1 (2023). <https://doi.org/10.1007/s41114-023-00043-4>. arXiv:1202.5809

19. V. Cardoso, P. Pani, Testing the nature of dark compact objects: a status report. *Living Rev. Rel.* **22**(1), 4 (2019). <https://doi.org/10.1007/s41114-019-0020-4>. arXiv:1904.05363
20. M. Reuter, Nonperturbative evolution equation for quantum gravity. *Phys. Rev. D* **57**, 971–985 (1998). <https://doi.org/10.1103/PhysRevD.57.971>. arXiv:hep-th/9605030
21. D. Dou, R. Percacci, The running gravitational couplings. *Class. Quant. Grav.* **15**, 3449–3468 (1998). <https://doi.org/10.1088/0264-9381/15/11/011>. arXiv:hep-th/9707239
22. D. Perini, Gravity and matter with asymptotic safety. *Nucl. Phys. B, Proc. Suppl.* **127**, 185–189 (2004). [https://doi.org/10.1016/S0920-5632\(03\)02428-9](https://doi.org/10.1016/S0920-5632(03)02428-9). arXiv:hep-th/0305053
23. R. Percacci, D. Perini, Asymptotic safety of gravity coupled to matter. *Phys. Rev. D* **68**, 044018 (2003). <https://doi.org/10.1103/PhysRevD.68.044018>. arXiv:hep-th/0304222
24. R. Percacci, D. Perini, Constraints on matter from asymptotic safety. *Phys. Rev. D* **67**, 081503 (2003). <https://doi.org/10.1103/PhysRevD.67.081503>. arXiv:hep-th/0207033
25. M. Reuter, F. Saueressig, Quantum gravity and the functional renormalization group: the road towards asymptotic safety, Cambridge University Press (2019)
26. A. Bonanno, M. Reuter, Renormalization group improved black hole space-times. *Phys. Rev. D* **62**, 043008 (2000). <https://doi.org/10.1103/PhysRevD.62.043008>. arXiv:hep-th/0002196
27. B. Koch, F. Saueressig, Structural aspects of asymptotically safe black holes. *Class. Quant. Grav.* **31**, 015006 (2014). <https://doi.org/10.1088/0264-9381/31/1/015006>. arXiv:1306.1546
28. A. Bonanno, M. Reuter, Cosmology with self adjusting vacuum energy density from a renormalization group fixed point. *Phys. Lett. B* **527**, 9–17 (2002). [https://doi.org/10.1016/S0370-2693\(01\)01522-2](https://doi.org/10.1016/S0370-2693(01)01522-2). arXiv:astro-ph/0106468
29. M. Reuter, H. Weyer, Renormalization group improved gravitational actions: A Brans-Dicke approach. *Phys. Rev. D* **69**, 104022 (2004). <https://doi.org/10.1103/PhysRevD.69.104022>. arXiv:hep-th/0311196
30. M. Reuter, H. Weyer, Running Newton constant, improved gravitational actions, and galaxy rotation curves. *Phys. Rev. D* **70**, 124028 (2004). <https://doi.org/10.1103/PhysRevD.70.124028>. arXiv:hep-th/0410117
31. C.-M. Chen, Y. Chen, A. Ishibashi, N. Ohta, Phase structure of quantum improved Schwarzschild-(Anti)de Sitter black holes. *Class. Quant. Grav.* **40**(21), 215007 (2023). <https://doi.org/10.1088/1361-6382/acfc91>. arXiv:2303.04304
32. O. Ruiz, E. Tuiran, Nonperturbative quantum correction to the Reissner-Nordström spacetime with running Newton's constant. *Phys. Rev. D* **107**(6), 066003 (2023). <https://doi.org/10.1103/PhysRevD.107.066003>. arXiv:2112.12519
33. R. Yang, Quantum gravity corrections to accretion onto a Schwarzschild black hole. *Phys. Rev. D* **92**(8), 084011 (2015). <https://doi.org/10.1103/PhysRevD.92.084011>. arXiv:1504.04223
34. X. Lu, Y. Xie, Weak and strong deflection gravitational lensing by a renormalization group improved Schwarzschild black hole. *Eur. Phys. J. C* **79**(12), 1016 (2019). <https://doi.org/10.1140/epjc/s10052-019-7537-2>
35. N. Kaiser, G. Squires, Mapping the dark matter with weak gravitational lensing. *Astrophys. J.* **404**, 441–450 (1993)
36. Y. Wang, A. Stebbins, E.L. Turner, Gravitational lensing of gravitational waves from merging neutron star binaries. *Phys. Rev. Lett.* **77**(14), 2875 (1996)
37. L.C.B. Crispino, D. Kennefick, 100 years of the first experimental test of General Relativity. *Nature Phys.* **15**, 416 (2019). <https://doi.org/10.1038/s41567-019-0519-3>
38. J.L. Synge, The Escape of Photons from Gravitationally Intense Stars. *Mon. Not. Roy. Astron. Soc.* **131**(3), 463–466 (1966). <https://doi.org/10.1093/mnras/131.3.463>
39. S.E. Gralla, D.E. Holz, R.M. Wald, Black Hole Shadows, Photon Rings, and Lensing Rings. *Phys. Rev. D* **100**(2), 024018 (2019). <https://doi.org/10.1103/PhysRevD.100.024018>. arXiv:1906.00873
40. V. Bozza, Gravitational lensing in the strong field limit. *Phys. Rev. D* **66**, 103001 (2002). <https://doi.org/10.1103/PhysRevD.66.103001>
41. R. Kumar, S.G. Ghosh, A. Wang, Gravitational deflection of light and shadow cast by rotating Kalb-Ramond black holes. *Phys. Rev. D* **101**(10), 104001 (2020)
42. S.U. Islam, R. Kumar, S.G. Ghosh, Gravitational lensing by black holes in the 4D Einstein-Gauss-Bonnet gravity. *JCAP* **09**, 030 (2020)
43. N.U. Molla, U. Debnath, Gravitational lensing for power-Maxwell charged quintessence black hole in Rastall gravity. *Int. J. Geom. Meth. Mod. Phys.* **19**(12), 2250183 (2022)
44. N. Tsukamoto, Gravitational lensing by a Bronnikov-Kim wormhole under a weak-field approximation and in a strong deflection limit. *Phys. Rev. D* **105**(6), 064013 (2022). <https://doi.org/10.1103/PhysRevD.105.064013>. arXiv:2111.13501
45. L. Angelini, L. Stella, A. Parmar, The discovery of 0.2 hz quasi-periodic oscillations in the x-ray flux of the transient 42 second pulsar exo 2030+ 375, *Astrophysical Journal, Part 1* (ISSN 0004-637X), vol. 346, Nov. 15, 1989, p. 906-911. 346 906–911 (1989)
46. R.V. Wagoner, A.S. Silbergleit, M. Ortega-Rodriguez, “stable” quasi-periodic oscillations and black hole properties from diskoseismology. *Astrophys. J.* **559**(1), L25 (2001)
47. M. Ortega-Rodríguez, H. Solís-Sánchez, L. Álvarez-García, E. Doderó-Rojas, On twin peak quasi-periodic oscillations resulting from the interaction between discoseismic modes and turbulence in accretion discs around black holes. *Mon. Not. Roy. Astron. Soc.* **492**(2), 1755–1760 (2020). <https://doi.org/10.1093/mnras/stz3541>. arXiv:1912.09527
48. Z. Stuchlík, M. Kološ, Mass of intermediate black hole in the source m82 x-1 restricted by models of twin high-frequency quasi-periodic oscillations. *Mon. Not. R. Astron. Soc.* **451**(3), 2575–2588 (2015)
49. M. Kološ, M. Shahzadi, Z. Stuchlík, Quasi-periodic oscillations around kerr-mog black holes. *Eur. Phys. J. C* **80**(2), 133 (2020)
50. M. Shahzadi, M. Kološ, Z. Stuchlík, Y. Habib, Epicyclic oscillations in spinning particle motion around kerr black hole applied in models fitting the quasi-periodic oscillations observed in microquasars and agns. *Eur. Phys. J. C* **81**(12), 1067 (2021)
51. M. Kološ, Z. Stuchlík, A. Tursunov, Quasi-harmonic oscillatory motion of charged particles around a schwarzschild black hole immersed in a uniform magnetic field. *Class. Quant. Gravit.* **32**(16), 165009 (2015)
52. M. Kološ, M. Shahzadi, A. Tursunov, Charged particle dynamics in parabolic magnetosphere around schwarzschild black hole. *Eur. Phys. J. C* **83**(4), 323 (2023)
53. Y. Liu, G. Mustafa, S. Maurya, F. Javed, Orbital motion and quasi-periodic oscillations with periastron and lense-thirring precession of slowly rotating einstein-æther black hole. *Eur. Phys. J. C* **83**(7), 584 (2023)
54. Y. Liu, G. Mustafa, S.K. Maurya, G. Yildiz, E. Gudekli, Testing of kerr black hole with quintessential dark energy through observational data by using quasi-periodic oscillations, Ertan, Testing of Kerr Black Hole with Quintessential Dark Energy Through Observational Data by Using Quasi-Periodic Oscillations
55. E. Tuiran, Quantum gravity effects in rotating black hole spacetimes, Ph.D. thesis, Mainz, Univ., Diss., 2007 (2007)
56. M. Reuter, E. Tuiran, Quantum Gravity Effects in the Kerr Spacetime. *Phys. Rev. D* **83**, 044041 (2011). <https://doi.org/10.1103/PhysRevD.83.044041>. arXiv:1009.3528
57. M. Reuter, Newton's constant isn't constant, 2000. arXiv:hep-th/0012069

58. J.M. Ladino, C.A. Benavides-Gallego, E. Larrañaga, J. Rayimbaev, F. Abdulxamidov, Charged spinning and magnetized test particles orbiting quantum improved charged black holes. *Eur. Phys. J. C* **83**(11), 989 (2023). <https://doi.org/10.1140/epjc/s10052-023-12187-2>. arXiv:2305.15350
59. J.F. Donoghue, Leading quantum correction to the Newtonian potential. *Phys. Rev. Lett.* **72**, 2996–2999 (1994). <https://doi.org/10.1103/PhysRevLett.72.299>. arXiv:gr-qc/9310024
60. J.F. Donoghue, General relativity as an effective field theory: The leading quantum corrections. *Phys. Rev. D* **50**, 3874–3888 (1994). <https://doi.org/10.1103/PhysRevD.50.3874>. arXiv:gr-qc/9405057
61. S. Chandrasekhar, The mathematical theory of black holes, In: *General Relativity and Gravitation: Invited Papers and Discussion Reports of the 10th International Conference on General Relativity and Gravitation*, Padua, July 3–8, 1983, Springer, pp. 5–26 (1984)
62. K.S. Virbhadra, G.F.R. Ellis, Gravitational lensing by naked singularities. *Phys. Rev. D* **65**, 103004 (2002)
63. C.-M. Claudel, K.S. Virbhadra, G.F.R. Ellis, The Geometry of photon surfaces. *J. Math. Phys.* **42**, 818–838 (2001)
64. V. Bozza, Gravitational Lensing by Black Holes. *Gen. Rel. Grav.* **42**, 2269–2300 (2010). <https://doi.org/10.1007/s10714-010-0988-2>. arXiv:0911.2187
65. V. Bozza, S. Capozziello, G. Iovane, G. Scarpetta, Strong field limit of black hole gravitational lensing. *Gen. Rel. Grav.* **33**, 1535–1548 (2001). <https://doi.org/10.1023/A:1012292927358>
66. V. Bozza, A Comparison of approximate gravitational lens equations and a proposal for an improved new one. *Phys. Rev. D* **78**, 103005 (2008). <https://doi.org/10.1103/PhysRevD.78.103005>. arXiv:0807.3872
67. K.S. Virbhadra, G.F.R. Ellis, Schwarzschild black hole lensing. *Phys. Rev. D* **62**, 084003 (2000). <https://doi.org/10.1103/PhysRevD.62.084003>
68. J. Kumar, S.U. Islam, S.G. Ghosh, Testing Strong Gravitational Lensing Effects of Supermassive Compact Objects with Regular Spacetimes. *Astrophys. J.* **938**(2), 104 (2022)
69. S. Gillessen, P. Plewa, F. Eisenhauer, R. Sari, I. Waisberg, M. Habibi, O. Pfuhl, E. George, J. Dexter, S. von Fellenberg et al., An update on monitoring stellar orbits in the galactic center. *Astrophys J* **837**(1), 30 (2017)
70. A. Einstein, Lens-Like Action of a Star by the Deviation of Light in the Gravitational Field. *Science* **84**, 506–507 (1936)
71. V. Bozza, L. Mancini, Time delay in black hole gravitational lensing as a distance estimator. *Gen. Rel. Grav.* **36**, 435–450 (2004)
72. C. Bambi, Black holes: a laboratory for testing strong gravity, Vol. 10, Springer (2017)
73. M.A. Abramowicz, W. Kluźniak, A precise determination of black hole spin in GRO J1655-40, aap 374 L19–L20 (2001). <https://doi.org/10.1051/0004-6361:20010791>. arXiv:astro-ph/0105077
74. J. Rayimbaev, S. Shaymatov, M. Jamil, Dynamics and epicyclic motions of particles around the schwarzschild-de sitter black hole in perfect fluid dark matter, *The. Eur. Phys. J. C* **81**, 1–12 (2021)
75. L. Stella, M. Vietri, S.M. Morsink, Correlations in the Quasi-periodic Oscillation Frequencies of Low-Mass X-Ray Binaries and the Relativistic Precession Model, *apjl* **524**, L63–L66 (1999). <https://doi.org/10.1086/312291>. arXiv:astro-ph/9907346
76. M. Bursa, High-frequency QPOs in GRO J1655-40: Constraints on resonance models by spectral fits, In: S. Hledík, Z. Stuchlík (Eds.), *RAGtime 6/7: Workshops on black holes and neutron stars*, pp. 39–45 (2005)
77. Z. Stuchlík, A. Kotrlová, G. Török, Multi-resonance orbital model of high-frequency quasi-periodic oscillations: possible high-precision determination of black hole and neutron star spin. *AAP* **552**, A10 (2013). <https://doi.org/10.1051/0004-6361/201219724>. arXiv:1305.3552
78. Frequency Correlation of QPOs Based on a Resonantly Excited Disk-Oscillation Model. *pasj* **60**, 889 (2008). <https://doi.org/10.1093/pasj/60.4.889>. arXiv:0803.2384